

The strength of nuclear shell effects at $N = 126$ in the r-process region

A.R. Farhan and M.M. Sharma
Physics Department, Kuwait University, Kuwait 13060
 (Dated: September 12, 2018)

We have investigated nuclear shell effects across the magic number $N = 126$ in the region of the r-process path. Microscopic calculations have been performed using the relativistic Hartree-Bogoliubov (RHB) approach within the framework of the Relativistic Mean-Field (RMF) theory for isotopic chains of rare-earth nuclei in the r-process region. The Lagrangian model NL-SV1 with the inclusion of the vector self-coupling of ω meson has been employed. The RMF results show that the shell effects at $N = 126$ remain strong and exhibit only a slight reduction in the strength in going from the r-process path to the neutron drip line. This is in striking contrast to a systematic weakening of the shell effects at $N = 82$ in the r-process region predicted earlier in the similar approach. In comparison the shell effects with microscopic-macroscopic mass formulae show a near constancy of shell gaps leading to strong shell effects in the region of r-process path to the drip line. A recent analysis of solar-system r-process abundances in a prompt supernova explosion model using various mass formulae including the recently introduced mass tables based upon Hartree-Fock-Bogoliubov method shows that whilst mass formulae with weak shell effects at $N = 126$ give rise to a spread and an overproduction of nuclides near the third abundance peak at $A \sim 190$, mass tables with droplet models showing stronger shell effects are able to reproduce the abundance features near the third peak appropriately. In comparison, several analyses of the second r-process peak at $A \sim 130$ have required weakened (quenched) shell effects at $N = 82$. Our predictions in the RMF theory with NL-SV1, which exhibit weaker shell effects at $N = 82$ and correspondingly stronger shell effects at $N = 126$ in the r-process region, support the conjecture that a different nature of the shell effects at the magic numbers may be at play in r-process nucleosynthesis of heavy nuclei.

PACS numbers: 21.10.Dr, 21.30.-x, 21.60.-n, 25.30.+k, 26.50.+x

I. INTRODUCTION

About half of nuclei heavier than Fe are synthesized in the process of rapid neutron capture (r-process) [1, 2, 3, 4, 5]. In environments of high neutron densities and high temperatures, extremely neutron-rich nuclei with at least 10-30 neutrons away from the stability line are produced. These nuclei are highly unstable and experimentally inaccessible, especially those in the heavy mass region. The ensuing nuclei undergo a sequence of neutron capture accompanied by a spate of β^- decays thus leading to formation of heavy elements in nature. The r-process path passes through the magic numbers $N = 50, 82$ and 126 at different mass values. The synthesis of nuclei around these magic numbers is reflected vividly in the known nuclear abundance peaks around $A \sim 80, 130$ and 190 , respectively.

The shell effects at the magic numbers play a significant role in determining the r-process nuclear abundances [4]. The question whether the shell effects near the r-process path are strong or do quench has become crucial to understanding the nucleosynthesis of heavy nuclei [6]. This question remains open to-date and the existing data do not suffice to answer this question. This is due to the reason that r-process nuclei are extremely neutron rich and are not accessible experimentally. Moreover, on the basis of a few nuclei that are known in the extreme regions, it is not easy to make reliable predictions in the farther regions of the period table. Consequently, it is proving to be difficult to ascertain the nature of the shell effects in the vicinity of the r-process path. A knowledge

about properties of these nuclei is, therefore, obtained from theoretical models. At the same time, new data in unknown regions are being obtained experimentally. Such data can be of enormous value in defining the nature of properties of nuclei in the extreme regions.

In principle, microscopic calculations within a reliable model would be attractive for the purpose. The primary condition on utility of a microscopic framework should be its ability to reproduce features and properties of nuclei in the known domains with better accuracy. Calculations within a microscopic model for a considerably large number of nuclei can be cumbersome. However, with the progress in computing speeds, such a task is no more beyond one's reach.

Heretofore, macroscopic-microscopic approaches have largely been used to calculate and extrapolate properties of nuclei in the inaccessible regions. Most prominent amongst these is the approach of the Finite-Range Droplet Model (FRDM) [7]. The mass formula FRDM has been obtained on the basis of extensive fits of more than a thousand known nuclei across the period table including those discovered at the periphery of the periodic table in the last decade. R-process calculations have been performed using the binding energies (masses) and neutron separation energies from the FRDM in conjunction with β -decay properties obtained in the Quasi-Particle Random Phase Approximation (QRPA) [8]. Another mass formula that has also been employed extensively is based upon the Extended Thomas-Fermi model with Strutinsky Integral (ETF-SI) [9]. Herein, the liquid drop (or the smooth) part is provided by the Extended

Thomas-Fermi model and the shell corrections are superimposed thereupon using the method of the Strutinsky shell correction [10].

Employing the results of these two mass formulae extensive r-process network chain calculations have been undertaken [4, 5, 6]. It was concluded that due to strong shell effects (gaps) at $N = 82$ and at $N = 126$ in the region of the r-process path inherent in the mass models FRDM and ETF-SI, strong deficiencies (troughs) are obtained in reproducing solar system r-process abundances below the peaks $A \sim 130$ and $A \sim 190$ [4, 6]. A remedial measure was suggested by the Hartree-Fock-Bogoliubov (HFB) calculations [11] using the Skyrme force SkP. This force is shown to quench (weaken) the strength of the shell effects in the r-process region significantly, especially at $N = 82$. This feature of HFB+SkP has proved to be useful in filling up the troughs below $A \sim 130$ and $A \sim 190$ in the r-process abundance curve. In this approach, the quenching effect is attributed mainly to a large effective mass $m^* = 1$ of the force SkP. Inspired by the usefulness of the quenching along the r-process path, contrary to the original feature of both the FRDM and the ETF-SI, quenching has been introduced in the new variant of the mass formula, viz., ETF-SI (Q) [12]. The mass table ETF-SI (Q) has been shown to be successful in removing the main deficiencies in the abundance curve [13]. These experiments with the mass formulae have indicated the need of weaker shell effects along the r-process path. A microscopic basis of such a requirement at the r-process path, however, needs to be examined.

In a recent investigation of the r-process nucleosynthesis of heavy nuclei using mass formulae based upon Hartree-Fock-Bogoliubov approach, it has been shown [14] that weak shell effects in microscopic mass formulae result in a spread of abundance distribution near the $A \sim 130$ and $A \sim 190$ peaks. This has the consequence that large deviations are observed compared to the solar-system abundances especially for the peak about $A \sim 190$. In an earlier analysis [15], it was also shown that in a realistic astrophysical scenario a mass model without quenching at $N = 126$ can fill up deficiencies (troughs) near $A \sim 175$ due to freeze-out effects. However, this seems to apply to only the third peak in the abundance curve. Thus, the role of the shell effects at $N = 126$ in the r-process region is not yet clear.

In our earlier work [16, 17, 18], we investigated the behaviour of the shell effects at the magic number $N = 82$ within the Relativistic Hartree-Bogoliubov approach. Using the Lagrangian model of the nonlinear quartic coupling of ω meson in the RMF theory, it was shown that microscopic RMF calculations show a weakening of the shell effects at $N = 82$ in going from the stability line to the r-process path. It was also shown that in going from the r-process path to the neutron drip line, the shell gap diminishes to a vanishingly low value at a given isospin, resulting in a complete washout of the shell effects [16]. In the present work, we have investigated the behaviour and evolution of the shell effects at $N = 126$

in the region of the r-process path within the framework of the RHB approach. The salient features of the formalism are discussed in Section III with emphasis on the shell properties of nuclei as inherent to the subject. Results of microscopic RMF calculations using two different Lagrangian models are presented in Section V. A comparison of the results is made with the predictions of various macroscopic-microscopic mass formulae and influence of shell effects on the r-process nucleosynthesis is discussed. A discussion is presented of the possible consequences of the shell effects on the r-process nucleosynthesis. A summary of the results is presented in the last section.

II. THE SHELL EFFECTS IN NUCLEI

The shell effects constitute an important feature of nuclei and are known to manifest strongly in terms of the magic numbers. This is signified by a conspicuous presence of prominent kinks about the major magic numbers in two-neutron separation energies (S_{2n}) all along the stability line [19]. This is a manifestation of the existence of large shell gaps at magic numbers in nuclei. The spin-orbit interaction plays a pivotal role in the creation of the shell gaps and consequently of the magic numbers. Of late, there are indications that with extreme isospin in light nuclei, re-adjustment of single-particle levels might lead to an emergence of new magic numbers [20] other than those which are hitherto established.

The spin-orbit interaction and consequently how the shell effects behave in the extreme regions would play a significant role in carving out shell gaps in nuclei near the r-process path. In microscopic approaches such as nonrelativistic density-dependent Skyrme theory and the relativistic mean-field theory, the spin-orbit interaction is determined by data on a few nuclei. Whilst in the former, the spin-orbit interaction is added in the theory on an *ad hoc* basis and its strength is adjusted to known spin-orbit splittings in a few nuclei, it arises naturally in the RMF theory as a consequence of the Dirac-Lorentz structure of nucleons. This has shown much usefulness in explaining properties that involve shell effects, such as anomalous isotope shifts in stable nuclei, especially those associated to the Pb chain [21]. This feature of the shell effects has not been possible to attain in the Skyrme theory without undertaking significant alterations in the isospin dependence of the spin-orbit interaction [22]. On the other hand, the intrinsic form of the spin-orbit interaction in the RMF theory has been found to be advantageous over that in the nonrelativistic approach. The appropriate isospin dependence of the spin-orbit interaction [23] has been found to be successful in reproducing the anomalous isotope shifts in Pb nuclei [21] as well as in Sr and Kr isotopes [24]. Consequently, it is expected to have implications in predicting the shell strength in the extreme regions of the r-process path.

The RMF theory [25, 26, 27, 28] has shown an im-

mense potential in being able to describe properties of nuclei along the stability line [29, 30] and for a large number of nuclei beyond the stability line. Most of the Lagrangian parameter sets are based upon reproduction of binding energies, charge radii and in some cases surface thickness of a few key nuclei [26]. Various forces are obtained in such a way that spin-orbit splitting in some key nuclei such as ^{16}O is reproduced reasonably well. It should, however, be pointed out that it does not necessarily ensure that shell gaps or shell effects at the major magic numbers are reproduced correctly.

The shell effects were not considered explicitly in the initial developments in the RMF theory of finite nuclei. This problem was addressed in Ref. [31], where shell effects were investigated in nuclei along the stability line with a view to see their influence on nuclei near r-process path or on some known “waiting-point” nuclei [16]. It was shown [31] that the otherwise successful RMF forces based upon non-linear self-coupling of σ -meson such as NL-SH [30] overestimate the experimental shell gaps in nuclei along the stability line. In order to solve this problem, the Lagrangian model with the nonlinear scalar coupling of σ meson was extended with the inclusion of the nonlinear quartic coupling of the ω meson [31]. Consequently, shell effects in Ni and Sn isotopes at the stability line were reproduced well.

The shell effects along the stability line (may) have repercussions (as it seems to be the case for the RMF theory, but not unequivocally for the mass formulae) on the shell effects far away from it. The character of the shell effects, be it strong or weak vis-a-vis experimental data along the line of stability is likely to extrapolate alike (unless major re-adjustments in single-particle scheme take place giving rise to unexpected pattern of behaviour) in the unknown regions of the periodic table. A test case for this hypothesis was provided by the waiting-point nucleus ^{80}Zn ($N = 50$) which lies close to the r-process path at $N = 50$. It was shown [16] that forces such as NL-SH that overestimate the shell effects at the stability line overestimate the shell effects for the waiting-point nucleus ^{80}Zn and also in r-process nuclei at $N = 82$. On the other hand, the force NL-SV1 based upon the vector self-coupling of ω -meson, which reproduces the shell effects in nuclei at the stability line, is able to reproduce the available data on the waiting-point nucleus ^{80}Zn [16]. A firmer verification of predictability of various theories would be provided by future experimental data in the extreme regions. In the present work, we explore how this feature translates for the shell effects at $N = 126$ in the r-process region.

III. THE RELATIVISTIC MEAN-FIELD THEORY

The RMF approach [25] is based upon the Lagrangian density which consists of fields due to various mesons interacting with nucleons. The mesons include the isoscalar

scalar σ -meson, the isoscalar vector ω -meson and the isovector vector ρ -meson. The details of the formalism can be found in Refs. [16, 26, 28, 29].

The RMF Lagrangian that describes the nucleons as Dirac spinors moving in the meson fields is given by [25]

$$\begin{aligned} \mathcal{L} = & \bar{\psi} \left(\not{p} - g_\omega \not{\omega} - g_\rho \not{\vec{\rho}} \vec{\tau} - \frac{1}{2} e(1 - \tau_3) \not{A} - g_\sigma \sigma - M_N \right) \psi \\ & + \frac{1}{2} \partial_\mu \sigma \partial^\mu \sigma - U(\sigma) - \frac{1}{4} \Omega_{\mu\nu} \Omega^{\mu\nu} + \frac{1}{2} m_\omega^2 \omega_\mu \omega^\mu \\ & + \frac{1}{4} g_4 (\omega_\mu \omega^\mu)^2 - \frac{1}{4} \vec{R}_{\mu\nu} \vec{R}^{\mu\nu} + \frac{1}{2} m_\rho^2 \vec{\rho}_\mu \vec{\rho}^\mu - \frac{1}{4} F_{\mu\nu} F^{\mu\nu} \end{aligned} \quad (1)$$

where M_N is the bare nucleon mass and ψ is its Dirac spinor. Nucleons interact with σ , ω , and $\vec{\rho}$ mesons, with the masses being m_σ , m_ω and m_ρ and the coupling constants being g_σ , g_ω , g_ρ , respectively. The electromagnetic interaction is represented by the electromagnetic vector field A^μ .

The field tensors for the vector mesons are given as $\Omega_{\mu\nu} = \partial_\mu \omega_\nu - \partial_\nu \omega_\mu$ and by similar expressions for the ρ -meson and the photon. For a realistic description of nuclear properties a nonlinear self-coupling

$$U(\sigma) = \frac{1}{2} m_\sigma^2 \sigma^2 + \frac{1}{3} g_2 \sigma^3 + \frac{1}{4} g_3 \sigma^4 \quad (2)$$

for σ -mesons has been widely used. The non-linear vector self-coupling of ω -meson [32] as added earlier [31] in the Lagrangian with the non-linear scalar field is represented by the coupling constant g_4 .

In the lowest order of the quantum field theory, i.e., in the mean-field approximation, the nucleons are assumed to move independently in the meson fields. The meson fields are replaced by their classical expectation values. The variational principle leads to the Dirac equation:

$$\{-i\alpha\nabla + V(\mathbf{r}) + \beta m^*\} \psi_i = \epsilon_i \psi_i \quad (3)$$

where $V(\mathbf{r})$ represents the *vector* potential:

$$V(\mathbf{r}) = g_\omega \omega_0(\mathbf{r}) + g_\rho \tau_3 \rho_0(\mathbf{r}) + \frac{e(1 - \tau_3)}{2} A_0(\mathbf{r}) \quad (4)$$

and $S(\mathbf{r})$ is the *scalar* potential

$$S(\mathbf{r}) = g_\sigma \sigma(\mathbf{r}) \quad (5)$$

which defines the effective mass as:

$$m^*(\mathbf{r}) = m + S(\mathbf{r}) \quad (6)$$

The Klein-Gordon equations for the meson fields are time-independent inhomogeneous equations with the nucleon densities as sources.

$$\begin{aligned} \{-\Delta + m_\sigma^2\} \sigma(\mathbf{r}) &= -g_\sigma \rho_s(\mathbf{r}) - g_2 \sigma^2(\mathbf{r}) - g_3 \sigma^3(\mathbf{r}) \\ \{-\Delta + m_\omega^2\} \omega(\mathbf{r}) &= g_\omega \rho_v(\mathbf{r}) + g_4 \omega^3(\mathbf{r}) \\ \{-\Delta + m_\rho^2\} \rho(\mathbf{r}) &= g_\rho \rho_3(\mathbf{r}) \\ -\Delta A(\mathbf{r}) &= e \rho_c(\mathbf{r}) \end{aligned} \quad (7)$$

The stationary state solutions ψ_i are obtained from the coupled system of Dirac and Klein-Gordon equations. The ground-state of the nucleus is described by a Slater determinant $|\Phi\rangle$ of single-particle spinors ψ_i ($i = 1, 2, \dots, A$). Solution of the Dirac equation is achieved by using the method of oscillator expansion [29]. In the RMF approach, the pairing is included within the BCS scheme. However, for the case of nuclei in the extreme regions of the r-process path and drip lines, the Fermi energy is very close to the continuum and many single-particle states couple to the continuum. Thus, the BCS method of pairing provides a crude approximation of such cases. The Relativistic Hartree-Bogoliubov (RHB) approach based upon quasi-particle scheme provides an appropriate framework to deal with nuclei of such a nature.

A. The Relativistic Hartree-Bogoliubov approach

Nuclei that are known to show strong pairing correlations are treated appropriately within the framework of the RHB approach. Pairing correlations in the neighbourhood of the Fermi energy in case of nuclei near r-process path and drip line become even more important. Herein, the RHB approach provides a suitable framework to deal with nuclei in the extreme regions.

It has been shown [34] that using Green's function techniques [35] a relativistic Hartree-Bogoliubov approach can be implemented using the Lagrangian as given above. Neglecting retardation effects and the Fock term, one obtains relativistic Dirac-Hartree-Bogoliubov (RHB) equations

$$\begin{pmatrix} h & \Delta \\ -\Delta^* & -h^* \end{pmatrix} \begin{pmatrix} U \\ V \end{pmatrix}_k = E_k \begin{pmatrix} U \\ V \end{pmatrix}_k, \quad (8)$$

where E_k are quasiparticle energies and the coefficients U_k and V_k are four-dimensional Dirac spinors normalized as

$$\int (U_k^\dagger U_{k'} + V_k^\dagger V_{k'}) d^3r = \delta_{kk'}. \quad (9)$$

The average field

$$h = \boldsymbol{\alpha} \cdot \mathbf{p} + g_\omega \omega + \beta(M + g_\sigma \sigma) - \lambda \quad (10)$$

contains the chemical potential λ . The meson fields σ and ω are determined self-consistently from the Klein Gordon equations as done in the case of the RMF equations discussed above with the scalar density $\rho_s = \sum_k \bar{V}_k V_k$ and the baryon density $\rho_v = \sum_k V_k^\dagger V_k$. The sum on k is taken only over the particle states in the no-sea approximation. The pairing potential Δ in Eq. (8) is given by

$$\Delta_{ab} = \frac{1}{2} \sum_{cd} V_{abcd}^{pp} \kappa_{cd} \quad (11)$$

The RHB equations (8) are a set of four coupled integro-differential equations for the Dirac spinors $U(r)$ and $V(r)$

that are obtained self-consistently. The RHB calculations are performed by expanding fermionic and bosonic wavefunctions in 20 oscillator shells. For the pairing channel, we use the finite-range Gogny force D1S [36]. The Gogny force is a sum of two Gaussians with finite range. It has been shown [36] that the Gogny force is able to describe pairing properties of a large number of finite nuclei in the medium and heavy mass regions. Details of the RHB theory can be found in Ref. [34]

B. Lagrangian Models

The Lagrangian model with the nonlinear scalar coupling of σ meson has been the widely used one for finite nuclei within the RMF theory. It has been successful in reproducing ground-state properties of nuclei at the stability line as well as of those far away from it. Here, we will consider the successful forces NL-SH [30] and NL3 [37] within this Lagrangian model. We will also employ the forces NL-SV1 and NL-SV2 [33] (see ref. [31] for the parameter sets) with the nonlinear vector self-coupling of ω meson. As mentioned above, forces NL-SV1 and NL-SV2 were constructed with the inclusion of the quartic vector coupling of ω meson, in order to solve the problem of strong shell effects with Lagrangian model with nonlinear scalar coupling of σ meson [31]. The introduction of the non-linear coupling of ω -meson also softens the equation of state (EOS) of the nuclear matter significantly. This has the consequence that the maximum neutron star mass with such an EOS would show a better agreement with empirically observed values. A detailed discussion of the properties associated with the introduction of the nonlinear vector self-coupling of ω meson in the RMF theory will be presented elsewhere [33]. It will be shown [33] that the Lagrangian parameter set NL-SV1 is also able to improve upon the ground-state properties such as binding energies, charge radii and isotopes shifts of nuclei along the stability line and far away from it as compared to those with NL-SH and NL3.

IV. DETAILS OF THE CALCULATIONS

In RHB calculations, wavefunctions are expanded into an harmonic-oscillator basis to solve the Dirac and the Klein-Gordon equations [29]. For both the fermionic and bosonic fields a basis of 20 oscillator shells has been used. The pairing has been taken in the Bogoliubov approach. For, nuclei a few neutrons below and a few neutrons above a magic number are usually spherical, RHB calculations have been performed for a spherical configuration. For a comparative study of the shell effects, we have performed RHB calculations with the two Lagrangian models as discussed above. However, our focus is on investigation of the potential and predictive power of the new Lagrangian model with the vector self-coupling of ω meson vis-a-vis the scalar self-coupling of σ meson.

With a view to investigate as to how the shell effects evolve in going from the region of the stability line towards the r-process path and ultimately to the neutron drip line, we have selected even-even nuclei from the isotopic chains of Hf ($Z = 72$) down to Xe ($Z = 54$) across the neutron magic number $N = 126$. For our focus is on the behaviour of the shell gap, nuclei relevant to the discussion are those with $N = 124$, $N = 126$ and $N = 128$, so as to be able to calculate S_{2n} values across the magic number $N = 126$.

V. RESULTS AND DISCUSSION

A. Shell effects along the stability line

First, we examine the known shell effects at $N = 126$ at the stability line. The experimental shell gap at $N = 126$ is known only in a very few isotopic chains in this region. Here, the doubly closed nucleus ^{208}Pb in the Pb chain provides a cardinal point in the study of the shell effects at $N = 126$. Interestingly, though the nuclear landscape of the periodic table has been extended significantly due to sustained experimental efforts in the last decade towards synthesizing nuclei far beyond the stability line in the laboratory, the heaviest known Pb nucleus has reached only to ^{214}Pb .

We begin with the premise that the two-neutron separation energy at the magic number provides a reasonably good indicator of the shell gap. Therefore, we calculate the shell gap at the magic number as defined conveniently by

$$\Delta_S = S_{2n}(Z, N_0) - S_{2n}(Z, N_0 + 2), \quad (12)$$

where $S_{2n}(Z, N_0)$ denotes the 2-neutron separation energy of the nucleus (Z, N_0) with a magic neutron number N_0 .

The shell gap in Pb nuclei obtained from the RMF approach using various Lagrangian sets is shown in Fig. 1(a) and (b). The corresponding gap from various macroscopic-microscopic mass formulae is shown in Fig. 1(c). The results are compared with the experimentally known data. The S_{2n} values calculated in the RMF theory with the forces NL-SH and NL3 within Lagrangian model of the nonlinear scalar coupling of σ meson are shown in Fig. 1(a). The difference between the data points at $N = 126$ and $N = 128$, as indicated by Eq. 12, manifests the shell gap at the magic number $N = 126$. A comparison with the experimental data points shows that the shell gap from the force NL-SH underestimates the experimental gap by ~ 0.5 MeV. On the other hand, the recent force NL3 shows a good agreement with the data. Here, we do not show the binding energy of ^{208}Pb itself that is overestimated both by NL-SH and NL3 by about 2-3 MeV. However, the difference in the S_{2n} values of the neighboring nuclei turns out to be satisfactory in both the cases. It is interesting to note that although

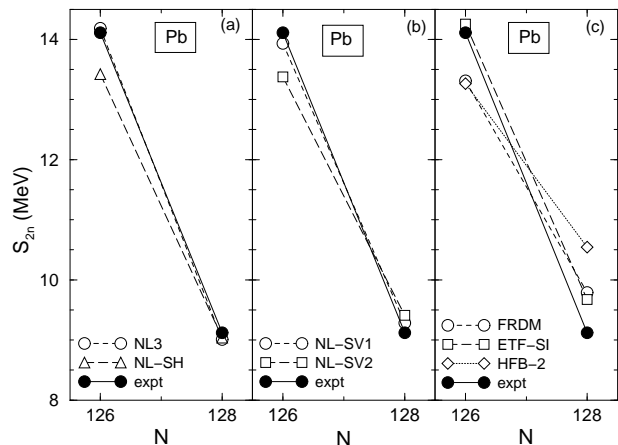


FIG. 1: The two-neutron separation energies S_{2n} for Pb isotopes as obtained from (a) the forces with the Lagrangian model of the nonlinear scalar self-coupling of σ meson, (b) from the forces which include the nonlinear quartic coupling of ω meson, and (c) from the mass formulae FRDM [7], ETF-SI [9] and the recently obtained results from mass tables HFB-2 [39]. The experimental data is shown by the solid circles.

NL-SH underestimates the shell gap at $N = 126$ slightly, it is known to exhibit generally stronger shell effects for nuclei at and beyond the stability line than those from NL3. This implies that a focus on a single or a few data points may not be deterministic as far as extrapolations (predictions) for nuclei beyond the stability line are concerned. Consequently, the shell gap at $N = 126$ in the Pb nucleus may not provide a successful conjecture as to whether the shell effects with either of the forces shall remain strong or weak in the domain that is far beyond the stability line.

The S_{2n} values obtained from the forces NL-SV1 and NL-SV2 with the Lagrangian model with the nonlinear quartic coupling of ω meson are shown in Fig. 1(b). A comparison with the experimental data shows that NL-SV1 reproduces the shell gap at $N = 126$ well, whereas it is underestimated by ~ 0.5 MeV by the force NL-SV2. Again, a seemingly paradoxical situation arises here. As in the case of NL-SH, exhibiting generally stronger shell effects and yet underpredicting the shell gap at $N = 126$ as shown in Fig. 1(a), the force NL-SV2 has also been shown to exhibit shell effects slightly stronger than those with NL-SV1 in the r-process region at $N = 82$ [16]. This shows that reliance on a few data points may not be useful in predicting behaviour in the extreme regions. This will be shown in the latter parts of this paper, where we will discuss the shell effects in the region of the r-process path and the neutron drip line.

It is equally interesting to see as to how various mass formulae predict the shell gap at $N = 126$ in Pb nuclei at the stability line. In Fig. 1(c), the data points from the mass formula FRDM and ETF-SI are shown. It may be remarked that various mass formulae including FRDM and ETF-SI have been obtained with a view to reproduc-

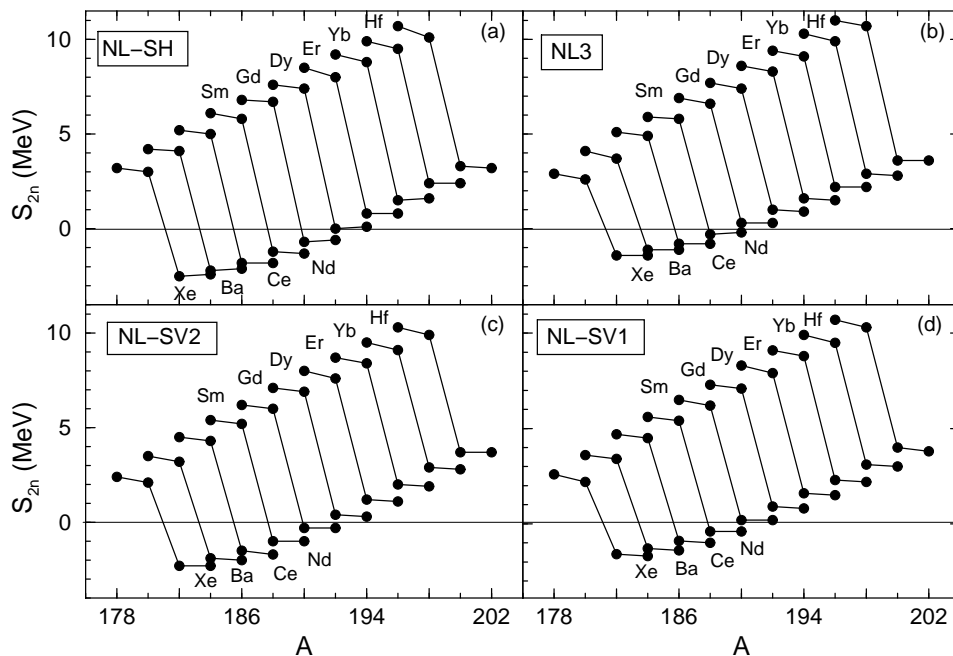


FIG. 2: The two-neutron separation energies S_{2n} for the isotopic chains from Hf ($Z = 72$) to Xe ($Z = 54$) in going towards the r-process nuclei and in approaching the neutron drip line, obtained from the forces with the Lagrangian model of the nonlinear scalar self-coupling of σ meson (a) NL-SH [30] and (b) NL3 [37]. The S_{2n} values from the forces which include the nonlinear quartic coupling of ω meson [31, 33] are also shown in (c) with NL-SV2 and in (d) with NL-SV1.

ing experimental data on more than a thousand nuclei. Generally, these mass tables have achieved a great success in reproducing a large set of experimental database through exhaustive fits over the periodic table than possibly a microscopic theory could ever do. However, as pointed out in the literature [7, 39], discrepancies at the magic numbers do remain a significant drawback.

The FRDM indicates a shell gap that is ~ 1.5 MeV smaller than the experimental one. On the other hand, ETF-SI underestimates the shell gap only by about 0.5 MeV. The undervaluation of the shell gap with FRDM and ETF-SI at $N = 126$ along the stability line is to be contrasted to the stronger shell effects due to these mass formulae when extrapolated in the extreme regions of the r-process path both at $N = 82$ and $N = 126$, than are suggested for a successful reproduction of r-process abundances. Notwithstanding the need of weaker shell effects along the r-process path, a new mass table based upon the Skyrme Hartree-Fock-Bogoliubov (HFB) approach has recently been produced [39]. The data points from the mass table HFB-2 as shown in Fig. 1(c) underestimate the shell gap at $N = 126$ significantly. It is worth pointing out that the mass formula HFB-2 [39] seems to have achieved a similar quality of fit across much of the periodic table. It is comparable to ETF-SI and FRDM, albeit with shell gaps that are predicted to be small in the r-process region, as we will see in Section V C.

B. Shell effects near the r-process path - RMF theory

The shell effects at $N = 126$ for r-process nuclei play a crucial role in determining r-process abundances around the peak at $A \sim 190$ [4]. For practical purposes r-process nuclei are defined to be those with $S_n \sim 2 - 4$ MeV. Thus, the r-process path is not strictly well defined and it does vary from model to model. However, it is generally accepted that nuclei with $Z \sim 64 - 69$ near $N = 126$ fall along the r-process path.

The results of RHB calculations for the forces NL-SH and NL3 with the Lagrangian model of nonlinear σ coupling are shown in the upper panels (a) and (b) of Fig. 2, respectively. It is seen clearly that the shell gap that is represented by the difference between the S_{2n} values at $N = 126$ and at $N = 128$ shows a gradual decrease with an increase in isospin i.e., in going from the element Hf ($Z = 72$) that is slightly above the r-process path to Xe ($Z = 54$) that is near the drip line. This behaviour is similar for both NL-SH and NL3. In absolute terms the shell gaps for NL-SH are slightly larger than those of NL3. However, in both the cases, the shell gap does not show a significant decrease in approaching the drip line, as is probably expected from a comparison with the corresponding behaviour of the shell gap at $N = 82$ along the drip line [16].

The S_{2n} values obtained from the forces NL-SV1 and NL-SV2 with the inclusion of quartic coupling of ω meson are shown in the lower panels (c) and (d) of Fig. 2, respec-

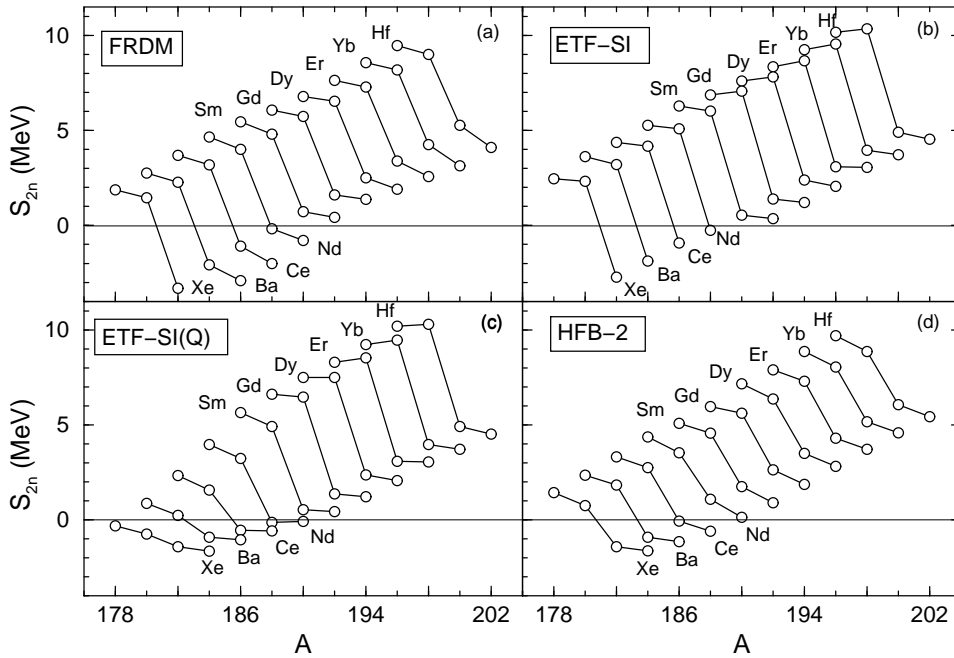


FIG. 3: The two-neutron separation energies S_{2n} for the isotopic chains from Hf ($Z = 72$) to Xe ($Z = 54$) in going towards the r-process nuclei and in approaching the drip line, as predicted by the mass models (a) FRDM [7] and (b) ETF-SI [9]. The S_{2n} values from the mass formula ETF-SI (Q) [12] that includes a quenching of the shell effects superimposed on ETF-SI are shown in (c). The results from the mass formula HFB-2 [39] are shown in (d).

tively. For both the forces NL-SV1 and NL-SV2, the shell gaps show a similar gradual decrease in going towards the r-process path and the drip line. Qualitatively, the behaviour of both the Lagrangian models as portrayed in the upper and the lower panels, respectively, is very similar. However, quantitatively, the shell gaps with NL-SV1 are smaller than both with NL-SH and NL3. The force NL-SV2 provides slightly larger shell gaps than those NL-SV1.

All the parameters sets of both the Lagrangian models exhibit a slight reduction in the shell strength in the region of the r-process path. The difference lies only in the degree by which the shell effects are reduced in going from the r-process path to the drip line. We will discuss the comparative behaviour of the shell effects with various RMF models in Section VD.

C. Shell effects near the r-process path - mass models

In the absence of and in essence rather infeasibility at present of constructing a mass table based purely on microscopic calculations, masses from various mass tables based upon macroscopic-microscopic approach are used in r-process calculations. Here, we present the results of the two most elaborate mass formulae, the FRDM and the ETF-SI.

We show the S_{2n} values obtained from the FRDM and ETF-SI in the upper panels (a) and (b) of Fig. 3, re-

spectively. In contrast to the microscopic calculations of Fig. 2, the shell gaps with FRDM and ETF-SI show nearly constant values in going from $Z = 72$ to $Z = 54$. On the other hand, a slight increase in the shell gap is visible with FRDM in going towards Xe. However, as the S_{2n} values from FRDM for the nuclides with $N = 128$ become negative below Nd ($Z = 60$), the apparent increase in the value of the shell gap for nuclei below Nd can be therefore be discounted.

A constant shell gap is also displayed by ETF-SI as shown in Fig. 3(b). The magnitude of the shell gap with ETF-SI, is, however, larger than that with FRDM by ~ 0.8 MeV. On the lower end, i.e., for nuclides with $N = 128$, the ETF-SI also shows negative S_{2n} values below Nd ($Z = 60$). Thus, the drip line is reached at $N = 128$ for the elements below Nd, the behaviour very similar to that of FRDM. Moreover, with ETF-SI the S_{2n} values for nuclides with the magic number ($N = 126$) are ~ 1 MeV larger than those of FRDM. The similar behaviour of the shell effects with FRDM and ETF-SI and arrival of the drip line at a similar location is not surprising, for the shell corrections superimposed on the smooth part in the two models are based upon the same prescription of the Strutinsky shell correction [10]

Predictions from the mass formulae FRDM and ETF-SI in the extreme regions of the r-process path have been used extensively for network chain calculations of r-process nuclear abundances. Results of calculations have shown that due to strong shell effects that are prevalent with FRDM and ETF-SI along the r-process path,

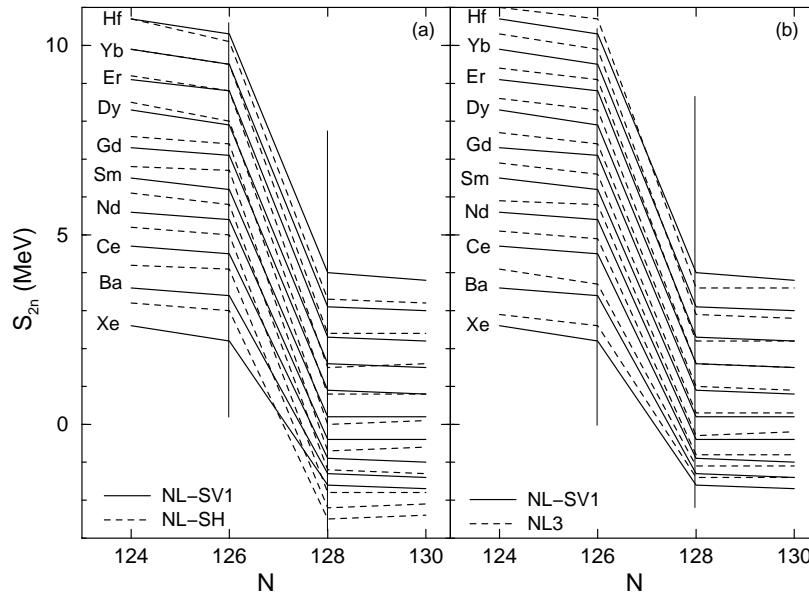


FIG. 4: The S_{2n} values from NL-SV1 are compared to those from (a) NL-SH and (b) NL3. The shell gap region is bounded by the two vertical lines at $N = 126$ and $N = 128$.

there is a significant deficiency (troughs) in the r-process abundances below the $A \sim 130$ and $A \sim 190$ peaks [4]. Inspired by the Hartree-Fock-Bogoliubov (HFB) calculations with the Skyrme force SkP [11], quenching was introduced in the ETF-SI mass formula, thus creating a new mass table ETF-SI (Q) [12]. The resulting r-process calculations [13] with ETF-SI (Q) have been able to fill up the deficiencies below the two peaks and results seem to be promising. This has put up a requirement (indirect) of a weakening of the shell structure for nuclei near the r-process path [13, 40]. This feature that is clearly absent in the original mass formulae FRDM and ETF-SI has been introduced in the ETF-SI (Q) rather artificially. The ETF-SI (Q) results in Fig. 3(c) show that the shell gaps remain the same as that with ETF-SI in going from Hf ($Z = 72$) to Er ($Z = 68$). However, the shell gap starts decreasing rapidly below Dy ($Z = 66$) in going towards Xe due to the quenching introduced therein. A microscopic basis of the aforesaid quenching introduced in the mass formula ETF-SI (Q) is yet to be established.

Motivated by the quenching present in the HFB calculations with SkP, attempts have been made to introduce the HFB approach in some mass tables. We show in Fig. 3 (d) the results taken from the recently developed mass table HFB-2 [39] within the Skyrme Ansatz. The shell gap with HFB-2 is reduced for all the isotopic chains as compared to FRDM and ETF-SI. A reduction in the shell gap with HFB-2 was also seen for Pb isotopes in Fig. 1(c). Though the shell gap is reduced vis-a-vis other mass formulae, it, however, remains constant in going from Hf ($Z = 72$) to Xe ($Z = 54$). There are no indications of an additional reduction in the shell strength near

the drip line as compared to the region of the r-process path. Thus, the constancy of the shell gap in going from the region of the r-process path to the drip line seems to be the salient feature of the macroscopic-microscopic mass tables presented in Fig. 3. Here, the only exception is ETF-SI (Q), wherein the quenching was introduced by force. In comparison, the RMF results show a slight reduction in the shell strength in going from the r-process path to the drip line.

An earlier version of the HFB mass table, i.e., HFB-1 was constructed by replacing the BCS pairing by the Bogoliubov pairing scheme in Ref. [41]. In this work, it was shown that the behaviour of shell gaps far away from the stability line does not depend much upon whether the BCS pairing or the Bogoliubov pairing is used. Accordingly, the shell gaps at $N = 126$ with HFB-1 were found to be comparable to those with FRDM and that an introduction of Bogoliubov pairing did not result in a quenching of the shell effects [41].

D. A comparative analysis of the shell effects

In order to understand the comparative behaviour of the shell effects first in the RMF theory, we show in Fig. 4 the S_{2n} values across the magic number $N = 126$ from the force NL-SV1 and compare these with the other forces such as NL-SH and NL3. It may be reminded that although the force NL-SH has been found to be successful in reproducing binding energies, charge radii and deformation properties of a large number of nuclei far away from the stability line, including the anomalous isotope

shifts in Pb nuclei, the shell effects with NL-SH were found to be stronger as compared to the experimental data [31]. In comparison, the force NL-SV1, having been able to describe the shell effects in Ni and Sn isotopes at the stability line, was also shown to be successful in reproducing the available data on the shell effects at the waiting-point nucleus ^{80}Zn [16]. In view of this, we treat the force NL-SV1 as our benchmark.

In Fig. 4(a), we compare the results of NL-SV1 to those from NL-SH. The variation in the shell gap is illustrated by the changing slopes of the curves between the vertical bars at $N = 126$ and $N = 128$. A look at the difference in the S_{2n} values and at the corresponding slope of the curve for Hf ($Z = 72$) shows that the shell gap with NL-SH is bigger than with NL-SV1. As one progresses towards the r-process nuclei such as Er, Dy, Gd and Sm, this difference in the shell gap between NL-SH and NL-SV1 increases with an increase in the isospin. One sees that the shell gaps with NL-SH remain stronger even in nuclei near the drip line such as Xe. In comparison, NL-SV1 shows a faster decrease in the shell gap in going from r-process nuclei to the drip line, a feature that has been called for for reproduction of r-process nuclear abundances.

The results from NL-SV1 are compared with those from the force NL3 in Fig. 4(b). A comparison between the shell gaps from the two forces shows that beginning with Hf, the shell gap with NL3 is slightly larger than that with NL-SV1. This difference, however, increases slowly when one moves from Hf to Xe. Thus, the shell effects with NL3 are slightly stronger than those with NL-SV1. Additionally, the S_{2n} values for nuclides with $N = 124$ are ~ 0.5 MeV higher with NL3 than NL-SV1, especially in the region of r-process nuclei. This feature is similar to that of NL-SH vis-a-vis NL-SV1 as shown in Fig. 4(a). We compare in Fig. 5 the shell gaps from NL-SV1 to those from the mass models (a) ETF-SI and from its variant (b) ETF-SI (Q) that embeds a quenching near the r-process region. For Hf ($Z = 72$), the shell gap with NL-SV1 is ~ 1 MeV larger than that of ETF-SI. However, as one proceeds to the r-process nuclei and towards the drip line, this difference between NL-SV1 and ETF-SI decreases and then it reverses. For drip line nuclei near Xe ($Z = 54$), the NL-SV1 shell gap is then smaller than that with ETF-SI. Whereas the shell gap with ETF-SI hardly shows any change in going from Hf to Xe, the shell gap with NL-SV1 does show a consistent decrease in going from the r-process to the drip line.

We also compare the NL-SV1 predictions to those of ETF-SI (Q) in Fig. 5(b). From the nuclei of Hf ($Z = 72$) to about Sm ($Z = 62$), there is not much difference between the results of ETF-SI and ETF-SI (Q). Therefore, for these nuclei, a comparison of NL-SV1 shell gaps with ETF-SI (Q) ones is similar to that with ETF-SI as shown in Fig. 5(b). In the region of r-process nuclei $Z = 64-68$, the shell gaps between NL-SV1 and ETF-SI (Q) are similar. However, due to an extra quenching added in ETF-SI (Q), differences in the shell gaps of the two approaches

begin appearing below $Z=62$. The shell gap with ETF-SI (Q) becomes especially small for nuclei near the drip line. The impact of the variations in the shell effects in nuclei can not be visualized without comprehensive r-process calculations. In the case of ETF-SI (Q), such calculations do exist and have shown promising results. On the other hand, r-process calculations using the results from NL-SV1 are being planned currently.

E. Models with strong shell effects

The strength of the shell effects at the major magic numbers has been a point of numerous discussions in respect of nuclear abundances [4, 5, 6]. The focus has mostly been on the possibilities and potential capabilities of various mass formulae of macroscopic-microscopic origin. This is evidently due to the fact that mass formulae have been able to produce large-scale nuclear binding energies and other data relevant for use in network chain calculations. The microscopic theories have not yet enjoyed this privilege with the exception of isolated case(s) where nuclear masses for the purpose have been calculated meaningfully. Here, we wish to take stock of the situation on the shell effects of nuclei within various frameworks.

We compare results of the mass formulae FRDM and ETF-SI, both of which show strong shell effects along with those from the RMF force NL-SH also exhibits strong shell effects. The S_{2n} values from FRDM and NL-SH are shown across the shell closure $N = 126$ in Fig. 6(a). The parallel lines for S_{2n} with FRDM from Hf to Xe in the the region of the shell gap bounded by the vertical lines in Fig. 6(a) indicate the constancy of the shell gap with FRDM as discussed above. The shell gap as indicated by the S_{2n} values from NL-SH and the ensuing large slope of the curve between $N = 126$ and $N = 128$ demonstrates overly strong shell effects with the force NL-SH. In comparison, the shell gap with FRDM is smaller than that with NL-SH by about 2 MeV for Hf nucleus. This difference between NL-SH and FRDM persists even for r-process nuclei in the region of $Z = 62-66$. Thus, the shell effects at $N = 126$ with NL-SH are significantly stronger than those with FRDM. However, due to natural decrease in the shell gap with an increase in isospin in the RMF theory, the shell gap with NL-SH does become comparable to FRDM for nuclei near the drip line.

The indication that the shell strength with NL-SH is strong appeared in Ref. [42], where the shell effects with NL-SH were studied across $N = 82$. In that work, it was shown that the shell effects at $N = 82$ with NL-SH were as strong as those with FRDM, but not stronger than FRDM. It was also shown that there was a remarkable agreement between the ground-state properties of the isotopic chains of Zr from ^{112}Zr through to ^{130}Zr in the two approaches. Nuclei in this region exhibited not only similar values of quadrupole deformation, but also

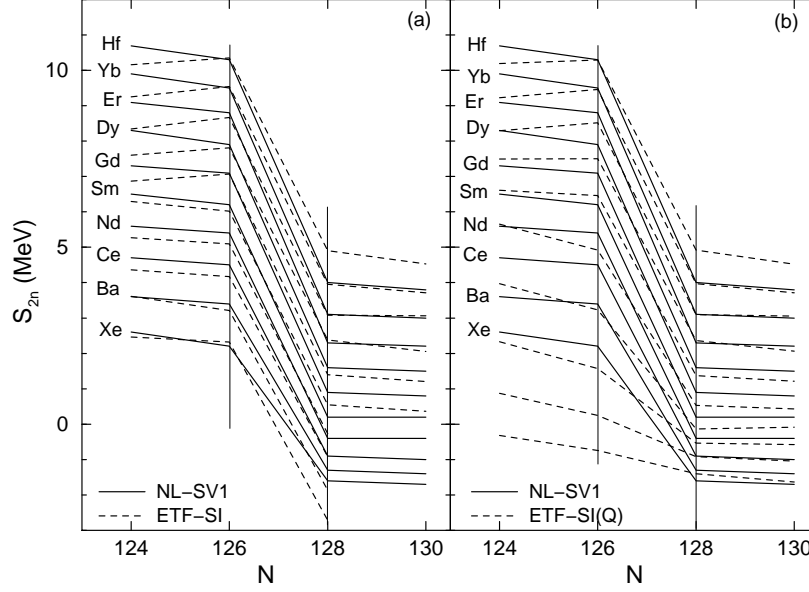


FIG. 5: The S_{2n} values from NL-SV1 are compared to those from the mass formula (a) ETF-SI and with the quenched mass formula (b) ETF-SI (Q). The shell gap region is bounded by the two vertical lines at $N = 126$ and $N = 128$.

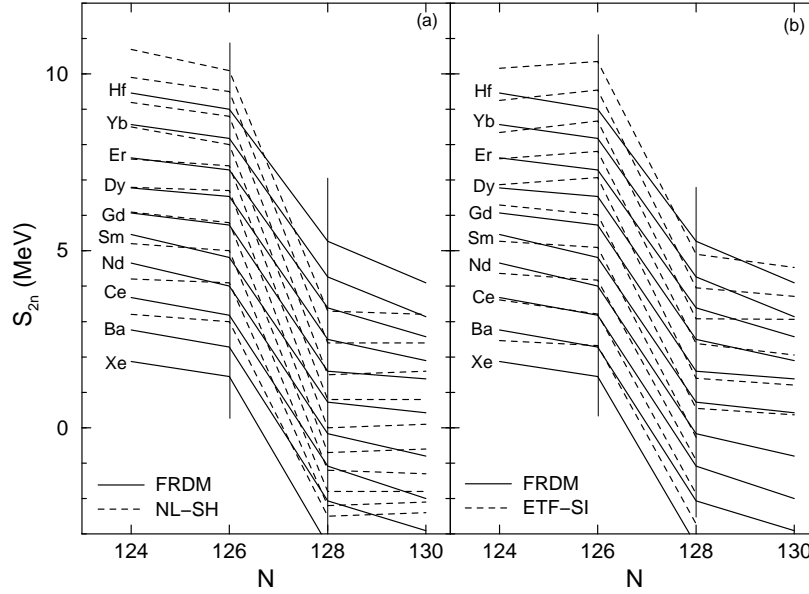


FIG. 6: The S_{2n} values from the FRDM are compared to those (a) from the force with strong shell effects NL-SH and (b) the mass formula with strong shell effects ETF-SI.

similar shape transitions across the region with FRDM and NL-SH [42]. This led to a surmise that the shell effects and shell structure with NL-SH are very similar to those of FRDM. However, this does not seem to be the case in the region of $N = 126$.

Taking into consideration the results of network chain calculations performed thus far, we believe that r-process network chain calculations with the force NL-SH or any

similar microscopic force exhibiting strong shell effects are not expected to be successful, at least for the third peak at $A \sim 190$.

We compare the shell effects with FRDM to those with ETF-SI in Fig. 6(b). The shell gaps with ETF-SI for nuclei in the vicinity of Hf are more than 1 MeV larger than those with FRDM. The strong shell gaps with ETF-SI are maintained across the r-process region and a near

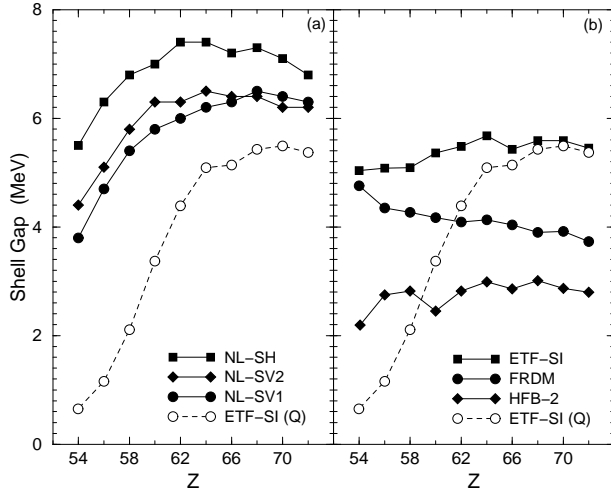


FIG. 7: The shell gaps Δ_S (Eq. 12) at $N = 126$ as obtained from the RMF forces (a) NL-SH, NL-SV1 and NL-SV2 and compared with those from ETF-SI (Q). (b) The shell gaps from mass formulae ETF-SI, FRDM and HFB-2 are shown. A comparison is also made with the ETF-SI (Q).

constancy of the shell gap at $N = 126$ both with FRDM and ETF-SI is seen clearly. The difference in the shell gap between ETF-SI and FRDM, however, decreases in going from the r-process path nuclei towards the drip line nuclei. The fact remains that with ETF-SI the shell effects are stronger than those with FRDM.

Using macroscopic-microscopic mass formulae FRDM and ETF-SI, it was shown [4, 15, 43] that due to the stronger shell gaps in ETF-SI, r-process network chain calculations lead to a greater deficiency (trough) in the r-process nuclear abundances below $A \sim 190$ peak than with FRDM. Thus, the earlier conclusion of much of these analyses has been that stronger shell effects at $N = 126$ do not seem to be conducive to reproducing nuclear abundances. However, it was shown in a later analysis [15] that in a “realistic” astrophysical scenario, there is no stringent need for a quenching of the $N = 126$ shell effects. The trough that appeared near $A \sim 175$ in earlier analyses could be filled due to freeze-out effects even by using a mass model without quenching. This raises the possibility that under appropriate conditions, mass formulae without a quenching of the shell strength at $N = 126$ can be used successfully.

F. The $N = 126$ shell gap in nuclei: RMF versus mass formulae

The status of $N = 126$ shell gaps Δ_S as defined in Eq. 12 is summarized in Fig. 7 for the RMF theory and for various mass formulae. The shell gap at $N = 126$ as obtained from the RMF calculations with NL-SH, NL-SV1 and NL-SV2 are shown in Fig. 7(a). All the microscopic calculations show a decreasing shell gap in going

through the r-process region. This reduction is, however, a little stronger as one moves towards the drip line.

A comparison shows that NL-SH exhibits shell gaps which are consistently larger than those with NL-SV1 and NL-SV2. This characterizes the stronger shell effects of NL-SH vis-a-vis other forces. The shell gaps with NL-SV2 are slightly larger than those with NL-SV1. This was also shown to be the case for shell gaps at $N = 82$ with NL-SV2 [16].

We compare the shell gaps with the RMF forces to those from the quenched mass formula ETF-SI (Q) in Fig. 7(a). Evidently, the shell gaps with ETF-SI (Q) are much smaller than those with NL-SH. However, these are also smaller than those of the NL-SV1 and NL-SV2. The effect of the added quenching in ETF-SI (Q) is apparent for nuclei below $Z = 64$, where the shell gap is reduced significantly as compared to the nearly constant values maintained in ETF-SI (see Fig. 7(b)). For nuclei below Nd ($Z = 60$), however, the quenching in the ETF-SI (Q) is much stronger than the weakening of the shell effects predicted by NL-SV1.

The shell gaps from various mass formulae are compared in Fig. 7(b). Both ETF-SI and FRDM exhibit shell gaps which remain nearly constant in going from the region of the r-process path towards the drip line. Comparatively, ETF-SI shows shell effects that are stronger than those with FRDM in much of the region shown in the figure. As shown in earlier calculations [13], the strength of the shell effects with ETF-SI was found to produce much larger deficiency below $A \sim 190$ peak in the r-process abundances.

The shell gaps with the new mass formula HFB-2 are compared with those from ETF-SI and FRDM in Fig. 7(b). The shell gaps with HFB-2 are nearly constant as shown also by the other mass formulae. These are, however, systematically smaller than those of ETF-SI and FRDM. There is a tendency of only a slight decrease in the shell gap in going towards the drip line nuclei. It is interesting to note that the addition of a Bogoliubov based pairing in the mass formula has not been found to be sufficient to suppress further the shell gaps below the r-process region. A comparison of the shell gaps from ETF-SI, FRDM and HFB-2 with those from ETF-SI (Q) shows that the shell gaps from ETF-SI (Q) are in striking contrast to all the other mass tables. However, as mentioned earlier, this striking difference has been brought about by the introduction of a quenching based upon results of HFB+SkP calculations. This extra weakening of the shell gaps in the drip line region is not shown by any of the widely used mass formulae. It has been reported in some calculations [12, 43] that a weakening of the shell effects in the r-process region to the drip line is required for reproducing the r-process abundances around the peaks at $A \sim 130$ and $A \sim 190$.

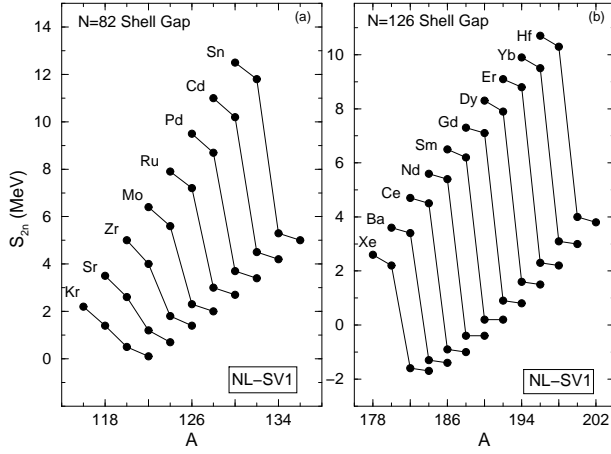


FIG. 8: The S_{2n} values from NL-SV1 are shown for nuclei across the shell closure (a) $N = 82$ and (b) $N = 126$ in the region of the r-process path. The evolution of the shell gaps at $N = 126$ is compared to that at $N = 82$.

G. The shell $N = 126$ versus $N = 82$

We discussed the evolution of the shell gap at $N = 82$ near the r-process path in the RMF theory in Ref. [16] in detail. The shell gaps at $N = 82$ were found to weaken in the region of the r-process path. In going to the drip line, the shell effects at $N = 82$ showed a substantial reduction in the shell strength, eventually leading to a complete disappearance of the shell gap for the drip line nuclei.

We show in Fig. 8 a comparison of the shell effects at $N = 126$ as obtained in the present work with those at $N = 82$ [16] in the region of the r-process path to the drip line. In order to visualize the shell gap at $N = 82$, we show the S_{2n} values obtained with NL-SV1 across the magic number for nuclides of Sn ($Z = 50$) down to the drip line nuclides of Kr ($Z = 36$). The shell gap at $N = 82$ shows a strong decrease in going from Cd ($Z = 48$) to Zr ($Z = 40$) in the region of the r-process path as mentioned above. This reduction in the shell gap at $N = 82$ is significantly faster than the corresponding shell gap at $N = 126$ (Fig. 8(b)). In the latter case, the shell gap shows a much slower decrease in the region of the r-process nuclei from Er ($Z = 68$) to Nd ($Z = 60$). The $N = 126$ shell strength exhibits a resilience to the change in isospin.

H. The shell effects and r-process nucleosynthesis

In the broader context of the shell effects and their implications on the r-process nucleosynthesis, it is pertinent to discuss recent r-process calculations which employ newly developed mass formulae HFB-2 and HFB-7 [14]. In this work, effect of various mass formulae on r-process nucleosynthesis has been studied using astrophys-

ical model of prompt supernova explosion from a collapsing O-Ne-Mg core [44]. In the mass formulae HFB-2 and HFB-7 which have been used, pairing has been taken into account by the Bogoliubov method in a Skyrme density-functional approach. R-process calculations in this study have also been carried out using the nuclear masses from FRDM [7] and from the old droplet mass (DM) model [45].

It has been shown [14] that due to the shell effects which are significantly reduced (weak) with HFB-2 and HFB-7, the abundance curve in the third peak at $A \sim 190$ is spread leading to a shift of the peak and consequently the valley at $A \sim 183$ is shifted significantly to lower masses. The results show that by the use of HFB-2 and HFB-7 masses, there are large deviations in the third peak as compared to the solar-system r-process abundances. Thus, due to the weakness of the shell effects at $N = 126$ near the r-process in the mass models HFB-2 and HFB-7, there is a significant overproduction of nuclei to the left of the third peak in the solar pattern. It is interesting to note that on using masses due to FRDM and DM, which are characterized by stronger shell effects at $N = 126$, it has been shown [14] that the abundance curve gives rise to a sharp r-process peak at $A \sim 190$, in better agreement with the solar pattern in the region. These results suggest that in the prompt supernova model considered in Ref. [14] and conditions applicable therein, mass models/microscopic theories with stronger shell effects at $N = 126$ would reproduce the main features of the solar r-process abundance curve around the third peak reasonably well. It may be recalled that rather similar conclusion was reached in Ref. [15], wherein it was shown that a mass model without quenching at $N = 126$ can fill up the trough at $A \sim 175$ and reproduce the abundance curve near the third peak due to freeze-out effects.

In view of the different behaviour of the shell effects at $N = 82$ and $N = 126$ as predicted by NL-SV1 in the RMF theory as shown in Fig. 8, it is pertinent to discuss the results of the r-process calculations of Ref. [14] around the second peak at $A \sim 130$. The results have shown that droplet mass models FRDM and DM with strong shell effects also at $N = 82$ produce troughs (underproduction) at $A \sim 115$ and $A \sim 140$ in the abundance curve. This shows that in contrast with $N = 126$, stronger shell effects at $N = 82$ are not desirable for reproducing the solar abundance pattern. On the other hand, with HFB-2 and HFB-7 deficiencies in the r-process production below and above the second peak at $A \sim 130$ are significantly remedied especially with HFB-2. However, the weak shell effects inherent in HFB-2 and HFB-7 have the consequence that abundances around $A \sim 130$ are also spread out as opposed to the solar system r-process abundances.

The results of Ref. [14] indicate that within the model employed in this work, the two peaks at $A \sim 130$ and $A \sim 190$ require a different nature of the shell effects. For a successful reproduction of abundances near $A \sim 130$,

shell effects at $N = 82$ in the r-process region should not be strong, whereas the third peak seems to require moderate to strong shell effects at $N = 126$ in contrast to $N = 82$. Thus, in the model considered in Ref. [14], the analysis of the second and the third peaks in the solar-system r-process abundance curve suggests a different nature of the shell effects at $N = 82$ and at $N = 126$.

Microscopic RHB calculations with the Lagrangian model NL-SV1 show two very different features for the shell effects at $N = 82$ and $N = 126$, as depicted in Fig. 8. These features seem to be consistent with the picture that emerges from the results of Ref. [14]. It remains to be seen in future network chain calculations with masses obtained from microscopic calculations with NL-SV1 whether the two different features of the shell effects exhibited by NL-SV1 would suffice towards reproducing the r-process abundances near the second and the third peak.

VI. CONCLUSIONS

We have investigated the shell effects in nuclei at the magic neutron number $N = 126$ in the region of the r-process path using the relativistic Hartree-Bogoliubov approach within the relativistic mean-field theory. Two Lagrangian models, one with the nonlinear scalar coupling of σ meson and another one that includes a nonlinear vector coupling of ω meson have been considered. A comparison of the shell effects in the RMF theory has been made with the predictions of various mass formulae. It is shown that the predictions of RMF calculations exhibit a slight reduction of the shell gap in going from the r-process path to the neutron drip line irrespective of the shell strength exhibited by a Lagrangian parameter set along the stability line. This is slightly different from a near constancy of the shell gaps demonstrated by major mass formulae in the region of the r-process path and the drip line. Consequences of the shell strength on

the r-process nucleosynthesis have been discussed.

It is shown that the Lagrangian force NL-SV1 with the vector self-coupling of ω meson, which reproduces the shell gaps along the stability line, shows that the shell effects at $N = 126$ exhibit only a marginal reduction in the shell strength in going from the r-process path to the drip line. Consequently, the shell effects retain a strong character along the r-process path at $N = 126$. This is in striking contrast to the earlier results [16] with NL-SV1 that in the RMF theory shell effects at $N = 82$ exhibit a significant weakening of the strength in going from the r-process path to the neutron drip line. This shows that different magic numbers may exhibit a different nature of the shell effects in the extreme regions of the periodic table.

Analysis of the results of a recent r-process calculations [14] has suggested that stronger shell effects at $N = 126$ and comparatively weaker shell effects at $N = 82$ are conducive to reproducing the r-process abundances in the second and the third peak, respectively, in the solar-system r-process abundance curve. Our results exhibit features which are consistent with this analysis and support the conjecture that a different nature of the shell effects may be at play in r-process nucleosynthesis of heavy nuclei.

A scrutiny of the shell effects with various RMF forces and with various mass formulae has shown that a given nature of the shell effects in a known region may not be sufficient to calibrate the shell structure in unknown regions. Accordingly, an extrapolation in the unknown regions of the r-process path is fraught with an uncertainty.

Acknowledgments

This work is supported by the Research project No. SP01/02 of the Research Administration, Kuwait University.

-
- [1] E.M. Burbidge, G.R. Burbidge, A.A. Fowler and F. Hoyle, *Rev. Mod. Phys.* **29**, 547 (1957).
 - [2] W. Hillebrandt, *Space Sci. Rev.*, **21**, 639 (1978).
 - [3] J.J. Cowan, F.-K. Thielemann, and J.W. Truran, *Phys. Rep.* **208**, 267 (1991).
 - [4] K.-L. Kratz, J.P. Bitouzet, F.-K. Thielemann, P. Möller, and B. Pfeiffer, *Astrophys. J.* **403**, 216 (1993).
 - [5] K.-L. Kratz, B. Pfeiffer, F.-K. Thielemann, and W.B. Walters, *Hyp. Int.*, **129**, 185 (2000).
 - [6] B. Pfeiffer, K.-L. Kratz, F.-K. Thielemann, and W.B. Walters, *Nucl. Phys.* **A693**, 282 (2001).
 - [7] P. Möller, J. Nix, W. Swiatecki, *At. Data Nucl. Data Tables* **59**, 185 (1994).
 - [8] P. Möller and J. Randrup, *Nucl. Phys.* **A514**, 1 (1990).
 - [9] Y. Aboussir, J.M. Pearson, A.K. Dutta and F. Tondeur, *At. Data Nucl. Data Tables* **61**, 127 (1995).
 - [10] V.M. Strutinsky, *Nucl. Phys.* **A122**, 1 (1968).
 - [11] J. Dobaczewski, W. Nazarewicz, T.R. Werner, J.F. Berger, C.R. Chinn, and J. Decharge, *Phys. Rev. C* **61**, 2809 (1996).
 - [12] J.M. Pearson, R.C. Nayak, and S. Goriely, *Phys. Lett. B* **387**, 455 (1996).
 - [13] B. Pfeiffer, K.-L. Kratz, and F.-K. Thielemann, *Z. Phys.* **A357**, 235 (1997).
 - [14] S. Wanajo, S. Goriely, M. Samyn and N. Itoh, *Astrophys. J.* **606**, 1057 (2004).
 - [15] F.K. Thielemann, K.L. Kratz, B. Pfeiffer, T. Rauscher, L. van Wormer and M.C. Wiescher, *Nucl. Phys.* **A570**, 329c (1994).
 - [16] M.M. Sharma and A.R. Farhan, *Phys. Rev. C* **65**, 044301 (2002).
 - [17] M.M. Sharma and A.R. Farhan, *Nucl. Phys.* **A688**, 353c (2001).
 - [18] A.R. Farhan and M.M. Sharma, *Nucl. Phys.* **A719**, 221c

- (2003).
- [19] C. Borcea, G. Audi, A. H. Wapstra, and P. Favaron, Nucl. Phys. A **565**, 158 (1993).
 - [20] J. Fridmann et al, Nature **435**, 922 (2005).
 - [21] M.M. Sharma, G.A. Lalazissis, and P. Ring, Phys. Lett. B **317**, 9 (1993).
 - [22] P.-G. Reinhard and H. Flocard, Nucl. Phys. **A584**, 467 (1995).
 - [23] M.M. Sharma, G.A. Lalazissis, J. König, and P. Ring, Phys. Rev. Lett. **74**, 3744 (1994).
 - [24] G.A. Lalazissis and M.M. Sharma, Nucl. Phys. A **586**, 201 (1995).
 - [25] B.D. Serot and J.D. Walecka, Adv. Nucl. Phys. **16**, 1 (1986).
 - [26] P.G. Reinhard, Rep. Prog. Phys. **52**, 439 (1989).
 - [27] B.D. Serot, Rep. Prog. Phys. **55**, 1855 (1992).
 - [28] P. Ring, Prog. Part. Nucl. Phys. **37**, 193 (1996).
 - [29] Y.K. Gambhir, P. Ring, and A. Thimet, Ann. Phys. (N.Y.) **198**, 132 (1990).
 - [30] M.M. Sharma, M.A. Nagarajan and P. Ring, Phys. Lett. B **312**, 377 (1993).
 - [31] M.M. Sharma, A.R. Farhan and S. Mythili, Phys. Rev. C **61**, 054306 (2000).
 - [32] A.R. Bodmer, Nucl. Phys. **A526**, 703 (1991).
 - [33] M.M. Sharma, in preparation (2005).
 - [34] H. Kucharek and P. Ring, Z. Phys. **A339**, 23 (1991).
 - [35] L.P. Gorkov, Sov. Phys. JETP **7**, 505 (1958).
 - [36] J.F. Berger, M. Girod and D. Gogny, Nucl. Phys. **A428**, 32 (1984).
 - [37] G.A. Lalazissis, J. König, and P. Ring, Phys. Rev. C **55**, 540 (1997).
 - [38] P. Möller, J.R. Nix, Nucl. Phys. **A536**, 221 (1992).
 - [39] S. Goriely, M. Samyn, P.-H. Heenen, J.M. Pearson and F. Tondeur, Phys. Rev. C **66**, 024326 (2002).
 - [40] B. Chen, J. Dobaczewski, K.-L. Kratz, K. Langanke, B. Pfeifer, F.-K. Thielemann, and P. Vogel, Phys. Lett. B **355**, 37 (1995).
 - [41] M. Samyn, S. Goriely, P.-H. Heenen, J.M. Pearson and F. Tondeur, Nucl. Phys. **A700**, 142 (2002).
 - [42] M.M. Sharma, G.A. Lalazissis, W. Hillebrandt, and P. Ring, Phys. Rev. Lett. **72**, 1431 (1994).
 - [43] K.-L. Kratz, in Nuclei in Cosmos III, AIP Conf. Proc. **327**, 113 (1995).
 - [44] S. Wanajo, M. Tamamura, N. Itoh, K. Nomoto, Y. Ishimaru, T.C. Beers, and S. Nozawa, Astrophys. J. **593**, 968 (2004).
 - [45] E.R. Hilf, H. von Groote, and K. Takahashi, in Proc. Third International Conference on Nuclei Far from Stability, (CERN), Geneva, p. 142.